ELECTRON SCATTERING EFFECTS IN TYPICAL COSMIC RAY TELESCOPES

J. E. Lupton* and E. C. Stone†
California Institute of Technology
Pasadena, California 91109

Abstract

Laboratory measurements have been made of the response of two typical cosmic ray detector systems to electrons between 0.2 and 2.0 MeV. The detector systems investigated were included in the Caltech Solar and Galactic Cosmic Ray Experiment aboard NASA's OGO-VI spacecraft and the Chicago/Caltech Low Energy Cosmic Ray Experiment aboard OGO-IV. Working laboratory versions of each of these particle telescopes were exposed to the monoenergetic electron beam from a magnetic spectrometer. The results of pulse height and counting rate measurements indicate that electrons scattered from the anti-coincidence cup comprise about 25% of the total number arriving at the top of the detector stack. In certain cases, the contribution of these scattered particles to the total number of electrons detected can reach 65%. Suggestions are made for applying these results to other detector systems.

Introduction

Although the problem of electron transport has been solved using Monte Carlo techniques[1,2,3], many specific electron problems can be solved easily only by direct experimental methods. This report grew out of a straightforward attempt to determine the response of two particular particle detection systems to an isotropic electron flux. In the process, it was found that the often-ignored contribution of electrons scattered from anti-coincidence shields was significant, and in one case, dominated the overall electron response of the system. The results, though admittedly specific to these particular telescope systems, should be useful for estimating the magnitude of such scattering effects in similar telescope systems.

The OGO-VI Cosmic Ray Telescope

The primary subject of this investigation is the ΔE-Range Telescope which is part of the Caltech Solar and Galactic Cosmic Ray Experiment aboard NASA's OGO-VI spacecraft. A description of the complete experiment, which consists of three cosmic ray telescopes and a common electronics package, has been published previously[4]. The Range Telescope shown in Figure 1 consists of seven totally-depleted silicon surface barrier detectors, five absorbers, and a cylindrical plastic scintillator anti-coincidence shield. The plastic scintillator is covered on the inside by an aluminum housing of .014" thickness. Individual energy-loss measurements are made in detectors D1, D2, and D3.

The low energy electron sensitivity of this telescope involves only detectors D1 through D3, since an incident electron energy of ∿ 6 MeV is needed to reach detector D4. Detector D1, because of its small depletion depth and high discriminator threshold[5], has an electron detection efficiency of less than 4×10^{-3}. Detectors D2 and D3, which in principle both have 100% electron detection efficiency, have incident energy thresholds of 0.2 and 1.1 MeV respectively. The Range Telescope characteristics are summarized in Table 1.

The Experiment

A working version of the Range Telescope system through detector D3 was constructed for laboratory use. A lucite cylinder covered on the inside with 0.015" aluminum was used to simulate the anti-coincidence shield. Because of its 0.7 MeV energy-loss threshold, the D8 shield rejects electrons scattering from its inner surface only at incident energies above 1.3 MeV. Thus, in our laboratory experiment the anti-coincidence shield was treated as a completely passive collimator and scattering surface.

Totally-depleted 1000 μm silicon surface barrier detectors were used to simulate D2 and D3; absorbers were used for D1 and A2. The pulse height signals from D2 and D3 were passed through charge-sensitive preamplifiers, shaping amplifiers, discriminators, count rate scalers, and in the case of D2, finally pulse-height analyzed. The physical dimensions, discriminator thresholds, and detector noise values of the actual OGO-VI flight unit were accurately reproduced in the laboratory version of the instrument.

A β-ray spectrometer employing a 10 mCi Sr^{90} source and a 2000 gauss electromagnet provided electrons up to a kinetic energy of 2 MeV. The electrons, which were extracted from the magnetic field, formed a unidirectional beam which varied in intensity by less than 10% over an area 2½" in diameter. The particles in this beam had an energy spread of less than 7% FWHM of the total energy. The total beam intensity was found to be contaminated approximately 10% by electrons of lower energy which were probably scattered from the spectrometer slits.

The laboratory prototype of the Range Telescope was mounted on a rotatable paddle and exposed to the electron beam as shown in Figure 2. The counting rates in D2 and D3 as well as the pulse height distribution in D2 were recorded for 18 different incident electron energies E_i and for 14 different angles of incidence θ_i. The raw data

* Now at Scripps Inst. of Oceanography, La Jolla, Calif.

† Alfred P. Sloan Research Fellow

can then be defined as functions of E_i, θ_i, and energy loss E':

$R2(E_i,\theta_i)$ = D2 counting rate in electrons/sec

$R3(E_i,\theta_i)$ = D3 counting rate in electrons/sec (1)

$P2(E',E_i,\theta_i)$ = energy loss distribution in D2 in electrons/sec-MeV

$N(E_i)$ = beam electron flux in electrons/cm^2-sec

An adjustable aluminum plate was included in the setup to shield the detectors from directly incident beam electrons. It was thus possible to directly measure the contribution of the electrons scattered from the scintillator cup, since only scattered electrons could reach D2 and D3 when the beam shield was in position. Data were recorded with and without the shield at all angles and energies, and thus determinations of the total response and the scattered response were made separately. The difference (total minus scattered) represents the response of the detectors to directly incident electrons. Note that a counting rate such as $R2(E_i,\theta_i)$, when normalized to the incident beam flux $N(E_i)$, becomes an effective detector area in cm^2.

Experimental Results

Since the raw data represented the telescope response to a unidirectional electron beam, it was possible to generate the response to an isotropic electron flux by integrating over angle as follows:

$$A\Omega_{D2}(E_i) = \frac{2\pi}{N(E_i)} \int_0^{\pi/2} R2(E_i,\theta_i) \sin\theta_i \, d\theta_i \qquad (2)$$

= effective D2 electron geometrical factor in cm^2 sr

In the same way

$$A\Omega_{D3}(E_i) = \frac{2\pi}{N(E_i)} \int_0^{\pi/2} R3(E_i,\theta_i) \sin\theta_i \, d\theta_i \qquad (3)$$

$$\frac{dA\Omega_{D2}}{dE'}(E',E_i) = \frac{2\pi}{N(E_i)} \int_0^{\pi/2} P2(E',E_i,\theta_i) \sin\theta_i \, d\theta_i \qquad (4)$$

= effective D2 electron geometrical factor per unit energy loss interval in cm^2 sr/MeV

Clearly one can also write

$$A\Omega_{D2}(E_i) = \int_{\text{D2 threshold}}^{\infty} \frac{dA\Omega_{D2}}{dE'}(E',E_i) \, dE'$$

as a simple check on the measurements.

The resulting values of $d(A\Omega_{D2})/dE'$ vs. energy loss E' are shown for 5 different incident energies in Figure 3. Note that for low incident energies, the scattered component forms a smooth spectrum slightly peaked at $E' \simeq 0.8\ E_i$. The effective electron geometrical factors for $D2\overline{D8}$ and $D3\overline{D8}$ are shown in Figure 4 broken down into scattered and directly incident components. Note that about 25% of the D2 response is due to scattered electrons. Since D2 has $\sim$ 100% detection efficiency for directly incident electrons, this 25% should approximate the number of scattered electrons reaching the detector surface relative to the total number.

The OGO-IV Telescope

A similar set of experiments was performed using the β-ray spectrometer described above in an effort to estimate the electron sensitivity of the Vertical Telescope of the University of Chicago/Caltech Low Energy Cosmic Ray Experiment aboard NASA's OGO-IV spacecraft. This telescope, shown in Figure 5, is very similar to the OGO-VI ΔE-Range Telescope. The OGO-IV telescope, however, has a much reduced electron detection efficiency due to smaller detector depletion depths and higher energy-loss discriminator thresholds. The characteristics of the Vertical Telescope are described in Table 2.

A working laboratory prototype of the OGO-IV telescope was constructed in a fashion similar to the OGO-VI simulation, except that the anti-coincidence cup was omitted. Spare flight detectors were used for both V1 and V2, and counting rates above a discriminator threshold were measured for each detector. For convenience, the spectrometer beam was collimated to a small cross-sectional area, and the responses due to directly incident and scattered electrons were determined in separate experiments. The scattering from the anti-coincidence cup was approximated in the laboratory by intercepting the spectrometer beam with a flat aluminum plate and then observing the counting rates in V1 and V2 detectors placed adjacent to this scattering plate. This technique required some knowledge of the geometrical factor of the anti-coincidence shield per unit incident angle ($dA\Omega/d\theta$), and also assumed that scattering from a plane is a reasonable approximation to the actual cylindrical geometry.

The results of this laboratory experiment are shown in Figure 6, which plots the effective electron $A\Omega$ for $V1\overline{V3}$ and $V2\overline{V3}$ as a function of incident energy. Note that the maximum OGO-IV

electron geometrical factors are respectively ∿ 7% and ∿ 23% of the AΩ for protons in contrast to ∿ 134% for the OGO-VI Range Telescope. Again, these electron efficiencies are a function of detector depletion depth and energy-loss threshold. Note also that in the case of V1, electrons scattered from the scintillator shield dominate the total response at incident energies above 700 keV. These scattering effects are considerably magnified in a detector which has a low efficiency for normally incident electrons, because the scattered particles, which enter the detector at oblique angles, have on the average a longer path length in the detector and thus a higher probability of being detected.

Conclusions

This experimental investigation, in addition to yielding information about the electron sensitivity of two specific cosmic ray telescopes, allows one to make some more general statements about contamination by electrons scattered from shields and collimators surrounding a detection system. This contamination is shown, for the present experiments, in Figure 7, which is a plot of the ratio of the scattered contribution to the total for $D2\overline{D8}$, $D3\overline{D8}$, $V1\overline{V3}$, and $V2\overline{V3}$. The results can be summarized as follows:

1. For particle telescopes with a configuration similar to that described above, roughly 25% of the electrons arriving at the surface of (but not necessarily detected by) the uppermost detector have been scattered from the inner walls of the anti-coincidence shield. This number should be roughly independent of the absolute size of the system as long as the relative sizes of the shield and detectors are preserved.

2. Because scattered electrons enter the detector stack at oblique angles, the effective detector thickness is greatly increased for these scattered particles. Thus, for detector systems with low electron detection efficiencies, the scattered particles are much more easily detected than the directly incident ones, and the contamination problem is enhanced. For instance, with the OGO-IV telescope a contamination level as high as 65% has been measured.

3. For detectors beneath absorbing layers, the relative contamination from the scattered electrons is decreased because the scattered particles are less capable of penetrating these layers than are the directly incident ones.

It is clear that the results shown in Figure 7 are quite easily explained in this light. These results and their interpretation should be helpful in defining the electron sensitivities of other particle telescopes.

Acknowledgments

This work was supported in part by the National Aeronautics and Space Administration under contract NAS5-3095 and NAS5-9312 and Grant Nos. NGR 05-002-160 and NGL 05-002-007. One of us (J.E.L.) has received valuable support from an NDEA Fellowship and a NASA Traineeship.

References

1. M. J. Berger and S. M. Seltzer, "Results of Some Recent Transport Calculations for Electrons and Bremsstrahlung," NASA SP-71, (1965).

2. M. J. Berger, S. M. Seltzer, S. E. Chappell, J. C. Humphreys, and J. W. Motz, "Response of Silicon Detectors to Monoenergetic Electrons with Energies Between 0.15 and 5.0 MeV," Nucl. Instr. and Methods, 69, 181, (1969).

3. C. D. Zerby and F. L. Keller, "Electron Transport Theory, Calculations, and Experiments," Nucl. Sci. and Eng., 27, 190, (1967).

4. W. E. Althouse, E. C. Stone, R. E. Vogt, and T. H. Harrington, "A Solar and Galactic Cosmic Ray Experiment," IEEE Trans. Nucl. Sci., 15, 229, (1967).

5. J. E. Lupton and E. C. Stone, "Measurements of Electron Detection Efficiencies in Solid State Detectors," Nucl, Instr. and Methods, in press.

Table 1. OGO-VI ΔE-Range Telescope

Detector/Absorber	Thickness mg/cm^2 (±3%)	Active Diameter cm (±3%)	AΩ Protons cm^2 sr (±6%)	Detector Noise σ in MeV (± .002)	Discriminator Threshold MeV (± .005)	Electron Threshold MeV
Window (Mylar)	2.3	-	-	-	-	-
D1 (Silicon)	22.1	1.60	1.1 ($D1\overline{D8}$)	0.038	0.40	-
D2 (Silicon)	233	2.20	1.8 ($D2\overline{D8}$)	0.020	0.15	∿ 0.20
A2 (Aluminum)	206	-	-	-	-	-
D3 (Silicon)	227	2.28	1.7 ($D3\overline{D8}$)	0.021	0.15	∿ 1.1

Table 2. OGO-IV Vertical Telescope

Detector/Absorber	Thickness mg/cm^2	Active Diameter cm (nom.)	AΩ Protons cm^2 sr	Detector Noise σ in MeV (± .002)	Discriminator Threshold MeV (± .02)	Electron Threshold MeV
Window (Mylar)	2.6 ± 0.2	-	-	-	-	-
V1 (Silicon)	106* ± 2	1.75	1.06 ($V1\overline{V3}$)	0.019	0.42	∿ 0.4
Absorber (Aluminum)	36 ± 4	-	-	-	-	-
V2 (Silicon)	133* (nom)	2.11	1.42 ($V2\overline{V3}$)	0.020	0.25	∿ 0.7
Absorber (Copper)	1790 ± 45	-	-	-	-	-

*V1 and V2 both have depletion depths of 56 ± 5 mg/cm^2

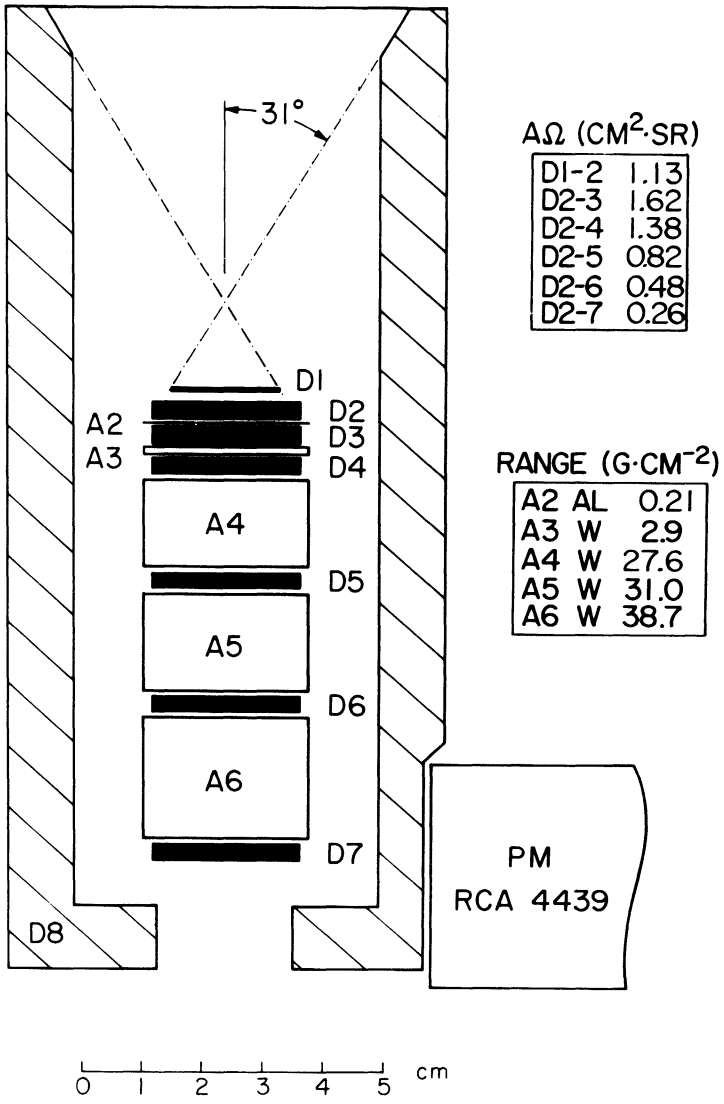

AΩ (CM^2·SR)

D1-2	1.13
D2-3	1.62
D2-4	1.38
D2-5	0.82
D2-6	0.48
D2-7	0.26

RANGE ($G \cdot CM^{-2}$)

A2	AL	0.21
A3	W	2.9
A4	W	27.6
A5	W	31.0
A6	W	38.7

Fig. 1 Cross-section drawing of the ΔE-Range Telescope aboard the OGO-VI spacecraft.

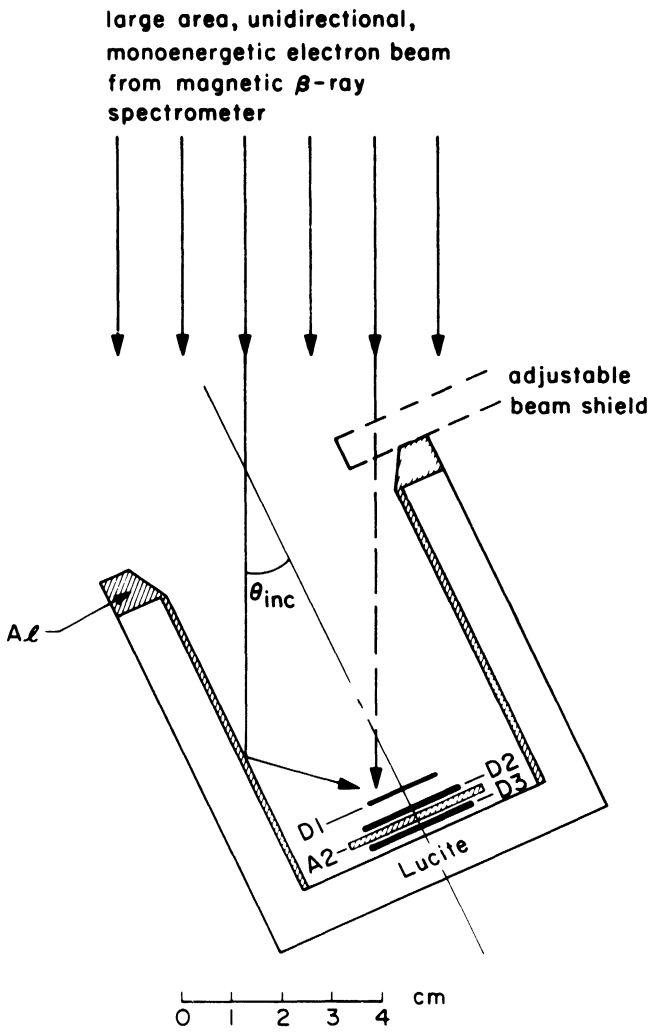

Fig. 2 Cross-section drawing of the laboratory set-up for determining the response of the OGO-VI ΔE-Range Telescope to electrons.

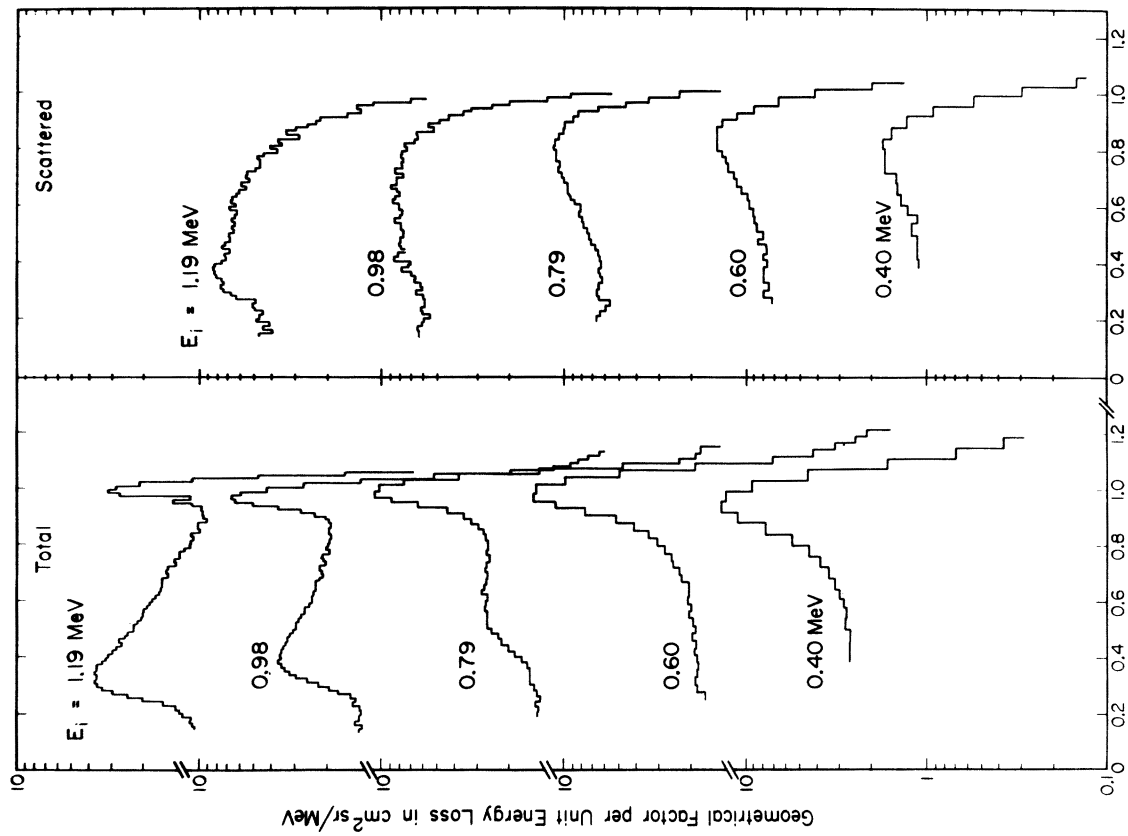

Fig. 3 Pulse height response of the OGO-VI D2 detector to an isotropic flux of monoenergetic electrons. The effective electron geometrical factor per unit energy loss interval $d(A\Omega_{D2})/dE'$ is plotted vs. normalized energy loss E'/E_i for 5 incident energies from 0.4 to 1.2 MeV. In each case, the total and the scattered electron contribution are shown separately.

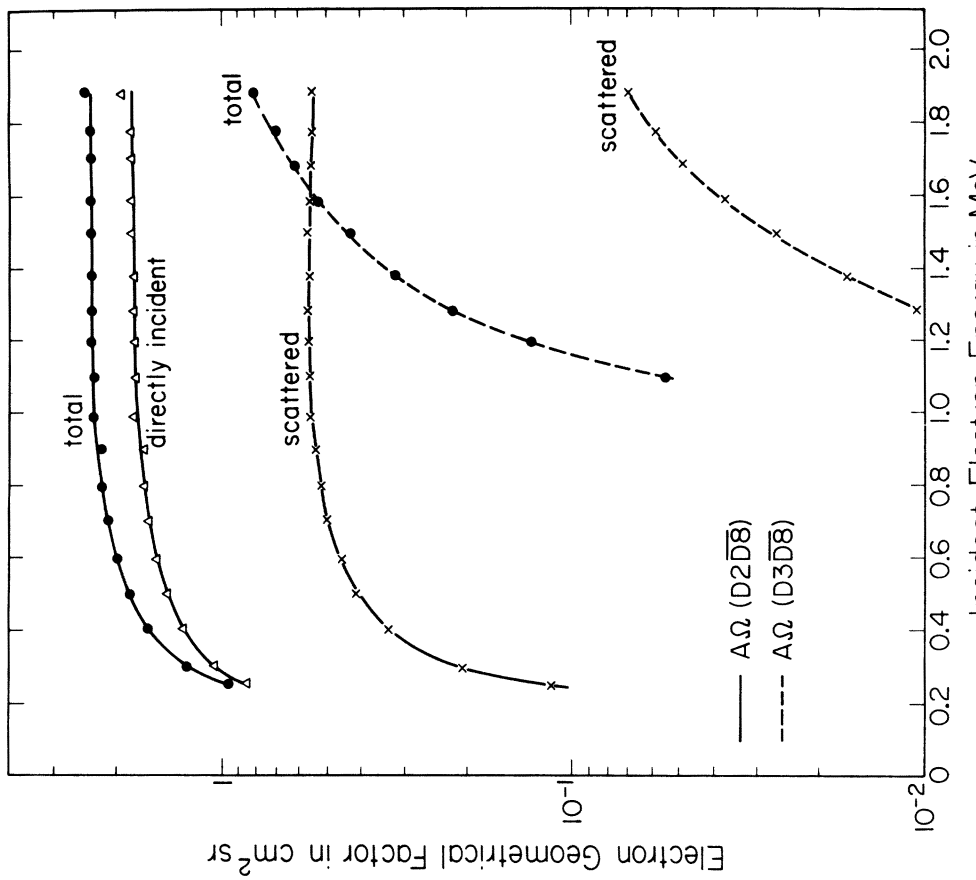

Fig. 4 The effective electron geometrical factor of the OGO-VI telescope for D2$\overline{D8}$ and D3$\overline{D8}$ events is plotted vs. incident electron energy. The contributions of directly incident and scattered electrons, as well as the total, are shown separately.

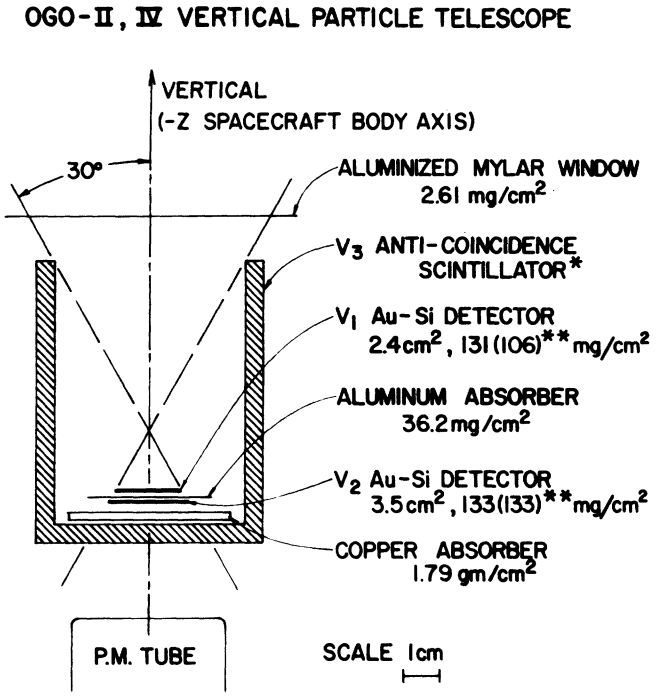

* SCINTILLATOR IS SURROUNDED BY 138 mg/cm² OF MAGNESIUM.

** VALUES FOR OGO-IV ARE IN PARENTHESES.

D_1 AND D_2 BOTH HAVE DEPLETION DEPTHS OF 56 mg/cm².

Fig. 5 Cross-section drawing of the Vertical Telescope aboard the OGO-IV spacecraft.

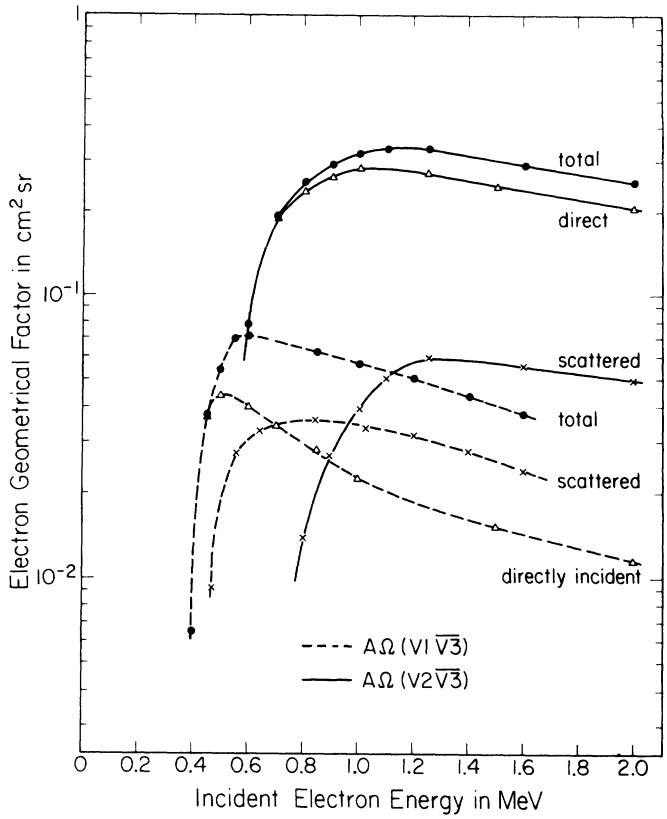

Fig. 6 The effective electron geometrical factor of the OGO-IV telescope for $V1\overline{V3}$ and $V2\overline{V3}$ events is plotted vs. incident electron energy. The contributions of directly incident and scattered electrons, as well as the total, are shown separately.

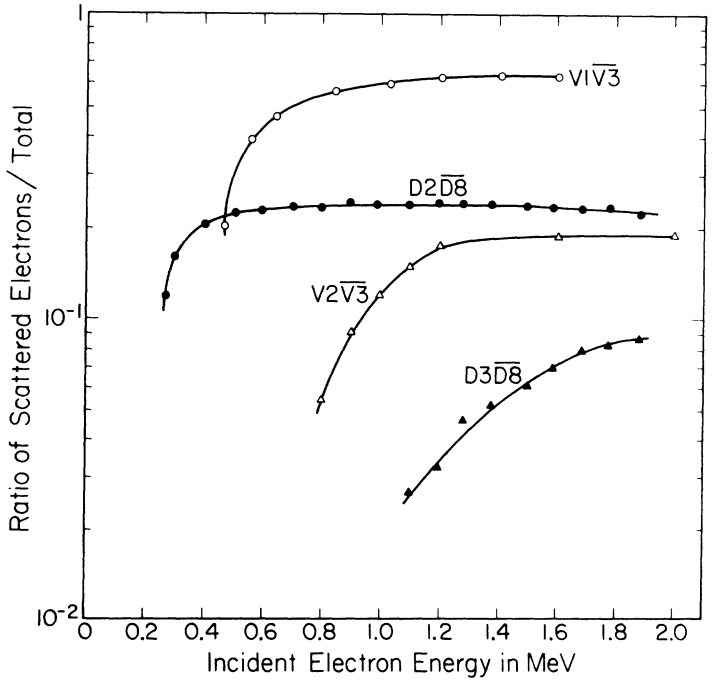

Fig. 7 Contamination of the total electron response by scattered electrons for both the OGO-VI and the OGO-IV telescope. The ratio of the scattered contribution to the total is plotted vs. incident electron energy for $D2\overline{D8}$, $D3\overline{D8}$, $V1\overline{V3}$ and $V2\overline{V3}$ events.